14. M. L. Moss and S. N. Greenberg, *Angle Orthod.* **37**, 151 (1967).
15. Y. Rak, *The Australopithecine Face* (Academic Press, New York, 1983).
16. M. L. Moss, *Acta Anat.* **44**, 263 (1961); S. W. Herring, *ibid.* **83**, 222 (1972); C. Katsaros, S. Killiardis, R. Berg, *Eur. J. Orthod.* **16**, 353 (1994).
17. M. A. McCollum, *Am. J. Phys. Anthropol.* **103**, 375 (1997).
18. A. Björk and V. Skieller, in *Factors Affecting the Growth of the Midface*, Monograph 6, *Craniofacial Growth Series*, J. A. McNamara Jr., Ed. (University of Michigan, Ann Arbor, MI, 1976), pp. 61–99; J. A. McNamara Jr., M. L. Riolo, D. H. Enlow, *Am. J. Phys. Anthropol.* **44**, 15 (1976); L. A. Bravo, I. L. Nielsen, A. J. Miller, *Am. J. Orthod. Dentofacial Orthop.* **96**, 26 (1989); E. D. Schneiderman, *Facial Growth in the Rhesus Monkey* (Princeton Univ. Press, Princeton, NJ, 1992).
19. T. G. Bromage, *J. Hum. Evol.* **18**, 751 (1989).
20. M. A. McCollum, *Am. J. Phys. Anthropol.* **93**, 259 (1994).
21. M. A. McCollum and S. C. Ward, *ibid.* **102**, 377 (1997).
22. G. C. Conroy and M. W. Vannier, *Nature* **329**, 625 (1987).
23. J. T. Robinson, *Am. J. Phys. Anthropol.* **12**, 181 (1954).
24. This model of robust australopithecine craniofacial morphogenesis predicts that the palatal component of the anterior nasal floor in *A. africanus* will display evidence of extensive resorption throughout growth. In the robust australopithecines, this same region should demonstrate reduced resorption later in cranial ontogeny. The predictions of this model are being assessed through scanning electron microscopic examination of the nasal cavity floor of juvenile australopithecine crania (*19*).
25. S. C. Ward and S. Molnar, *Am. J. Phys. Anthropol.* **53**, 383 (1980).
26. I thank O. Lovejoy, T. White, G. Suwa, and T. Bromage for comments on the manuscript, D. Knopsnyder for assistance with the graphics, and L. Gudz for providing original artwork. This research was supported by grants from Sigma Xi and the Boise Fund.

3 November 1998; accepted 3 March 1999

Solar Cycle Variability, Ozone, and Climate

Drew Shindell,[1]* David Rind,[1] Nambeth Balachandran,[1] Judith Lean,[2] Patrick Lonergan[3]

Results from a global climate model including an interactive parameterization of stratospheric chemistry show how upper stratospheric ozone changes may amplify observed, 11-year solar cycle irradiance changes to affect climate. In the model, circulation changes initially induced in the stratosphere subsequently penetrate into the troposphere, demonstrating the importance of the dynamical coupling between the stratosphere and troposphere. The model reproduces many observed 11-year oscillations, including the relatively long record of geopotential height variations; hence, it implies that these oscillations are likely driven, at least in part, by solar variability.

It has long been speculated that long-term solar output variations influence Earth's climate and may have caused episodes such as the Little Ice Age. As surface temperatures have risen rapidly over recent decades, it has become increasingly crucial to determine the relative importance of solar variation on climate. A first step is understanding the effects of the well-observed 10- to 12-year activity cycle. Although many meteorological quantities are correlated with the solar cycle (*1, 2*), it has remained unclear how relatively small changes in solar radiation (~0.1%), whose direct effects occur predominantly in the upper atmosphere, could have an important impact on Earth's surface. Cosmic ray influence on clouds has been proposed (*1*); others have suggested that the variability reflects other influences such as volcanoes (*3*) or internal climate oscillations (*4*). Another proposed mechanism is amplification of solar variability via stratospheric or thermospheric changes (*5, 6*). Measurements show that 10 to 20% of solar cycle irradiance changes occur in ultraviolet (UV) radiation (*7*), which is largely absorbed by stratospheric ozone.

A problem has been that most models with which this question has been studied have had limited stratospheric representations, have assumed a constant change in solar irradiance at all wavelengths, or have assumed constant ozone concentrations (*8–10*). Results showed that UV absorption changes altered the upper stratospheric zonal wind, which in turn affected planetary wave propagation and hence the troposphere. However, surface changes were quite small unless input solar variation was unrealistically large. One recent model (*6*) showed that incorporating both realistic solar irradiance and ozone changes could increase the response to solar forcing, but this model extended only to the middle stratosphere (10 mbar), a limitation that restricted the model's ability to simulate planetary wave propagation (*11*).

Here, we include both realistic irradiance and ozone changes in a climate model with a complete stratosphere. We used the GISS stratospheric general circulation model (GCM), a primitive equation model including parameterized gravity waves (*10*), with 8° latitude by 10° longitude resolution and 23 levels extending from the surface to 85 km (0.002 mbar). The two-dimensional (2D) model–derived chemistry parameterization includes wavelength-dependent ozone response to changes in radiation and temperature (*12*). Solar variability directly affects both ozone photochemistry and local heating, modifying ozone abundances, which in turn further alter local heating rates as well as the radiation field at other levels.

The GCM was run for 20 years each at solar maximum and solar minimum irradiances specified by wavelength-dependent changes from 180 to 400 nm, and constant changes at longer wavelengths consistent with total solar cycle irradiance variations (*7*). Results were analyzed in two ways: for the entire 40 years, and for a subset of the 28 years without sudden stratospheric warmings. The model showed no significant difference in generation of sudden warmings between phases, in accordance with observations (*13*). A companion experiment used identical radiation changes and constant ozone. All simulations had fixed sea-surface temperatures and no quasi-biennial oscillation (that is, the model was in its base state with weak easterlies).

Geopotential heights are controlled by temperatures in the underlying column, in addition to surface pressures, and thus height changes reflect temperature modification throughout the atmosphere below. An observed 10- to 12-year oscillation is present in more than 40 years of data (*2, 14*). Heights from about 10° to 50°N are well correlated with solar flux [>99.9% significance at 30 mbar for the annual average zonal mean (*2*)]. We concentrate on December through February, when differences in observed height changes between Northern Hemisphere subtropical and high latitudes are the greatest (between 30° and 90°N, a change of 104 m in winter versus 33 m in summer).

The individual years of the solar maximum and minimum simulations were averaged to reduce the noise, then the difference between them was calculated. The zonal mean 30-mbar height changes showed significant increases at low and mid-latitudes (Fig. 1). An additional experiment with ozone changes prescribed according to observations gave a similar response to that with calculated ozone, indicating the robustness of the result. The models with solar forcing and interactive ozone reproduce observed Northern Hemisphere subtropical height increases well, but the model with solar forcing and with constant ozone does not. For compari-

[1]NASA Goddard Institute for Space Studies (GISS) and Center for Climate Systems Research, Columbia University, 2880 Broadway, New York, NY 10025, USA. [2]E. O. Hulburt Center for Space Research, Naval Research Laboratory, Washington, DC 20375, USA. [3]Space Science and Applications Inc., 2880 Broadway, New York, NY 10025, USA.

*To whom correspondence should be addressed. E-mail: dshindell@giss.nasa.gov

son, a model with volcanic aerosols, another candidate for causing the observed variations, shows a very different pattern, with a distinct minimum at Northern Hemisphere mid-latitudes. That run did not include heterogeneous chemistry-induced ozone variations resulting from changes in aerosol loading (*3*); however, because those aerosol changes would induce large decreases at northern mid-latitudes (*15*), they would likely worsen the agreement between the modeled and observed height changes.

Restricting the analysis to years without sudden warmings does not substantially alter the results except at high latitudes, where extremely large variability renders both the model results and the observations statistically insignificant when sudden warmings are included. In any case, the high-latitude height differences in the analysis without warmings are significantly different from zero but are not significantly different from the 40-year analysis, which provides a better match to the observations, or from the observations themselves. Because the restricted analysis improves the signal-to-noise ratio (the results from all 40 years are statistically significant only from 22° to 38°N), we concentrate on that analysis. The similarity between the responses with and without sudden warmings is evidence that the signal does not merely reflect this natural mode of variability.

Throughout the Northern Hemisphere, the temperature response of the lower atmosphere to solar increases causes elevated subtropical and mid-latitude geopotential heights and decreased heights near the pole (Fig. 2). The model reproduces the overall pattern of height increases across all longitudes, although with a somewhat reduced magnitude, suggesting that the observed pattern may indeed arise from solar forcing. At lower levels, such as 100 mbar, the model again reproduces observed patterns, which are quite similar to those at 30 mbar.

Ozone transport differences were calculated noninteractively (*12*) because of limitations in computer resources. In the model, solar cycle–induced circulation changes increased ozone by 1 to 2% from about 25° to 30°N, at 50- to 90-mbar altitude during Northern Hemisphere winter. Additional increases occurred from 0° to 20°N below 100 mbar, whereas ozone decreased slightly (0.5 to 1.5%) from 35° to 50°N. Because additional ozone leads to greater heating, inclusion of these changes would bring the 30-mbar geopotential height changes (Fig. 1) even closer to the observations by raising values from 0° to 30°N and decreasing them at higher latitudes. As also shown from observations (*16*), transport changes affect lower stratospheric ozone and should be included interactively when resources permit.

During other seasons, the model's response is consistently weaker than observed (although observations show a much weaker response than the December–February period) and shows minimal statistical significance. The signal may simply be too weak to extract, or this may reflect model limitations, including the lack of variable sea surface temperatures, the quasi-biennial oscillation, and interactive ozone transport.

The physical causes of the simulated height changes are revealed by examining the GCM's behavior. Calculated ozone changes, based on our 2D model–derived parameterization, are similar to those found in earlier 2D models (*17*) (Fig. 3). Although models agree with the measured variations at 30 mbar (~26 km), satellite observations show much larger ozone differences above ~40 km (*18, 19*). Observations cover less than two solar cycles, however, and were perhaps affected by the two large volcanic eruptions that occurred during the data period

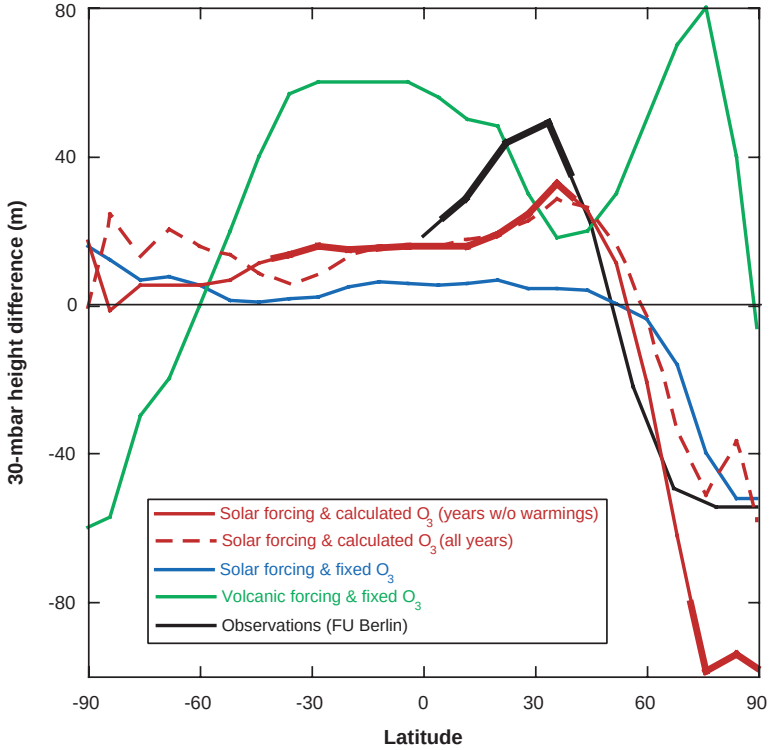

Fig. 1. Modeled zonal mean differences in December–February 30-mbar geopotential heights between solar maximum and solar minimum in GISS GCM runs with interactive ozone, both for the entire simulation and for only those years without sudden warmings (*23*), and with constant ozone. Also shown are results from a simulation with Pinatubo-like volcanic forcing (*24*). In that simulation, sea surface temperatures were allowed to adjust, so the results are taken from only the first 3 years (a rough lifetime for volcanic aerosols injected into the stratosphere). Thick portions of lines indicate statistical significance (>90%) for the interactive ozone run and for 40 years of observations (*2*). In the region where the observations are statistically significant, the results from the calculated ozone experiment are within the uncertainty of the observations for both analyses.

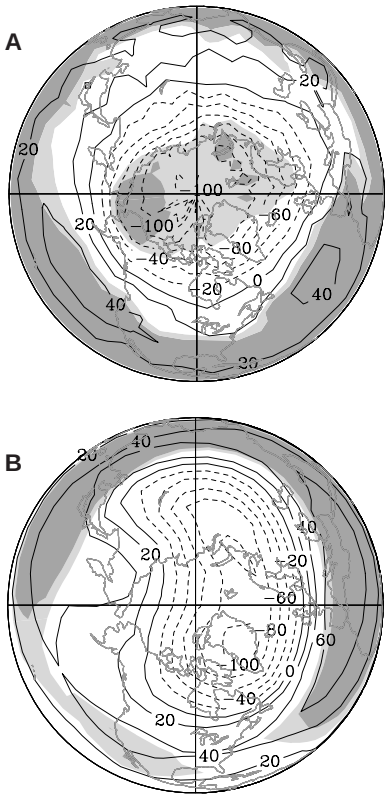

Fig. 2. December–February 30-mbar geopotential height differences between solar maximum and solar minimum for years without stratospheric warmings (**A**), and in the observations (as in Fig. 1) (**B**) (*2*). The shading shows 90% (light) and 95% (dark) significance levels.

near successive solar maxima (*3*).

During Northern Hemisphere winter, modeled ozone increased by about 2 to 4% in the middle stratosphere (Fig. 4A). Southern Hemisphere ozone increases were smaller because increased chemical destruction induced by temperature increases offset radiation-induced increases, as seen in earlier 2D models (*17*). Ozone changes in the dark polar region were those from when sunlight was present, and were "frozen in" once polar night began and photochemistry ceased. Increases in ozone abundance and incoming UV radiation lead to greater UV absorption and hence greater solar heating during solar maximum (Fig. 4B). The largest increases occurred in the Southern Hemisphere, where the received radiation change was greatest, and above the largest ozone increases.

Increased solar heating broadly warmed the Southern Hemisphere middle and upper stratosphere during December–February (Fig. 5). Observations also show general stratospheric warming above ~35 km, and maxima in the upper stratosphere and in the summer hemisphere (*18*). Modeled changes in the lower atmosphere and at high northern latitudes result from indirect dynamical changes induced by the solar variation.

The solar heating differences increased the middle and upper stratospheric latitudinal temperature gradient, enhancing the December zonal wind from 30° to 50°N by more than 4 m s^{-1} (Fig. 5). The resulting decreased horizontal shear of the zonal wind at these latitudes (*20*) increased the quasi-geostrophic potential vorticity and hence the index of refraction for planetary waves [as seen in earlier GCMs (*9, 10*)]. In some regions, the index of refraction changed from negative to positive (45° to 60°N, 20 to 5 mbar). Tropospheric wave energy is then less able to propagate into the middle stratosphere at northern mid-latitudes, and instead propagates preferentially toward lower latitudes. This resulted in a heating divergence in the polar lower stratosphere and convergence and warming in the lower stratosphere at mid-latitudes (Fig. 5). As angular momentum transport is in general opposite in direction to wave energy propagation, northward transport of angular momentum increased in the upper troposphere. The resulting greater divergence of angular momentum transport at mid-latitudes induced a circulation cell with a descending branch at ~40°N and an ascending branch at ~60°N. By February, the troposphere and lowermost stratosphere cooled at high northern latitudes, and warmed around 25° to 45°N (both are statistically significant), because of the more southerly convergence of wave energy and the induced circulation cell, creating the mid-latitude ridge seen in the geopotential heights. Thus, solar variability affects the troposphere indirectly by affecting how the troposphere distributes its own energy.

Both observations and previous GCM simulations support this mechanism. GCM studies (*9, 10, 21*) showed that Eliassen-Palm flux convergence changes associated with shifts in wave propagation lead to the downward propagation of the wintertime zonal wind increase, as in Fig. 5. The resultant strong February dipole pattern is clearly visible in observations (*14, 21*), although it is slightly larger in magnitude. However, the observations only cover a single solar cycle. The tropospheric mid-latitude zonal wind increase (Fig. 5) caused a slight poleward shift in the Northern subtropical jet, as also seen in observations (*21*). Haigh (*6*) found a similar shift, suggesting that our simulated response is not unique to the GISS GCM.

In comparison, the simulation with constant ozone showed roughly two-thirds the solar heating changes of the interactive ozone run, and only half the northern high-latitude upper stratospheric dynamical heating, suggesting that wave propagation was affected similarly, but not as severely as in the interactive run. Differences in the lower stratosphere were even greater, with a maximum December–February average high-latitude cooling of only –0.7 K (instead of –2.4 K),

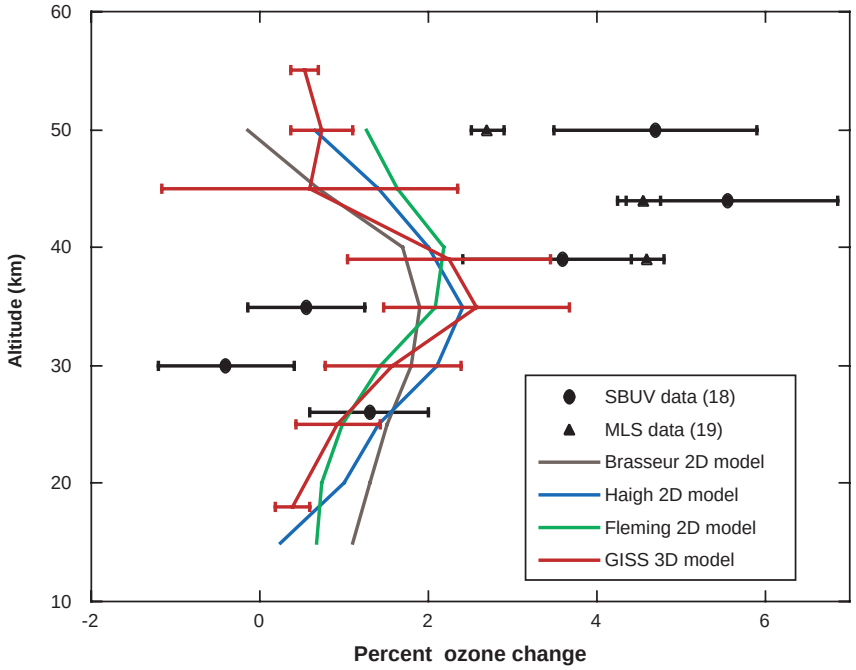

Fig. 3. Annual average percentage ozone differences between solar maximum and solar minimum averaged from 60°S to 60°N. The data points are from satellite observations covering 15 years for Solar Backscatter Ultraviolet (SBUV) data (*18*) and 3 years for Microwave Limb Sounder (MLS) data (*19*). The lines give results from the indicated models, including ozone-temperature feedbacks. GISS results are from the GCM, including our 2D model–derived parameterizations of ozone photochemistry.

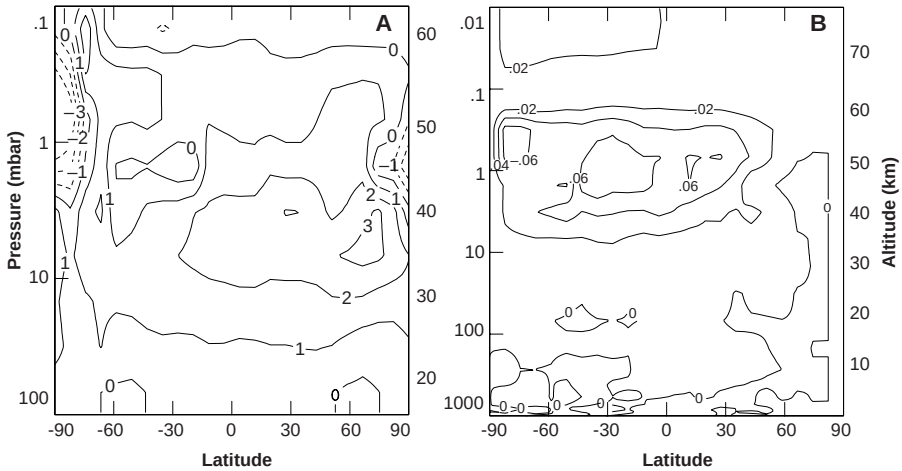

Fig. 4. Percent ozone differences (**A**) and solar heating differences in kelvin per day (**B**) between solar maximum and solar minimum calculated in the GISS GCM for the December–February period. Values are zonal means on a latitude by height plot. Decreases are shown with dashed lines. Note that (A) and (B) have different vertical scales.

and no evidence of the subtropical lower stratospheric–upper tropospheric warming of the interactive ozone simulation. Stratospheric ozone feedback therefore plays a crucial role in the amplification process whereby solar heating variations modify zonal wind, altering wave propagation, which then alters the equator-to-pole energy transport that largely governs the lower atmosphere's temperature response.

The tropospheric circulation changes affect surface meteorology. However, surface variability is much larger than that in the stratosphere, so that neither modeled nor observed surface changes are generally statistically significant. Nevertheless, the simulated tropospheric changes are generated by the statistically significant stratospheric changes via dynamical coupling, so it is likely that they are somewhat realistic.

Solar cycle forcing affects surface winds and sea level pressures. The statistically significant zonal mean zonal wind increase shown in Fig. 5 for February results from two large regional patterns. An increase in pressure over the northeastern Pacific increases the anticyclonic flow, bringing warmer air from lower latitudes over Canada. A similar effect occurs over the North Atlantic and over northern Eurasia, bringing warmer air up over the Arctic Ocean in the Eastern Hemisphere. The result is zonal mean surface warming of up to 0.5 K northward of 55°, and cooling (up to ~0.2 K) from about 35° to 55°N. A similar pattern, showing the largest temperature response at northern high latitudes over land, was seen previously (*8*). Zonal mean sea level pressure increases ~0.7 mbar from 30° to 45°N, with an associated decrease of ~1.1 mbar from 75° to 85°N, greater in magnitude than (though quite similar in location to) that reported by Haigh (*6*).

Solar cycle variability may therefore play a significant role in regional surface temperatures, even though its influence on the global mean surface temperature is small (0.07 K for December–February). The radiative forcing of the solar cycle, resulting from both irradiance changes and the impact of greenhouse trapping by the additional ozone, is also small (0.2 W m^{-2} for December–February). Although the 11-year solar cycle is relatively short, the use of variable sea surface temperatures would perhaps affect the results. Another consideration is that upper stratospheric ozone has decreased significantly since the 1970s as a result of destruction by halogens released from chlorofluorocarbons (*22*). This ozone decrease, which has been much larger than the modeled solar-induced ozone increases, may have limited the ability of solar irradiance changes to affect climate over recent decades, or may have even offset those effects.

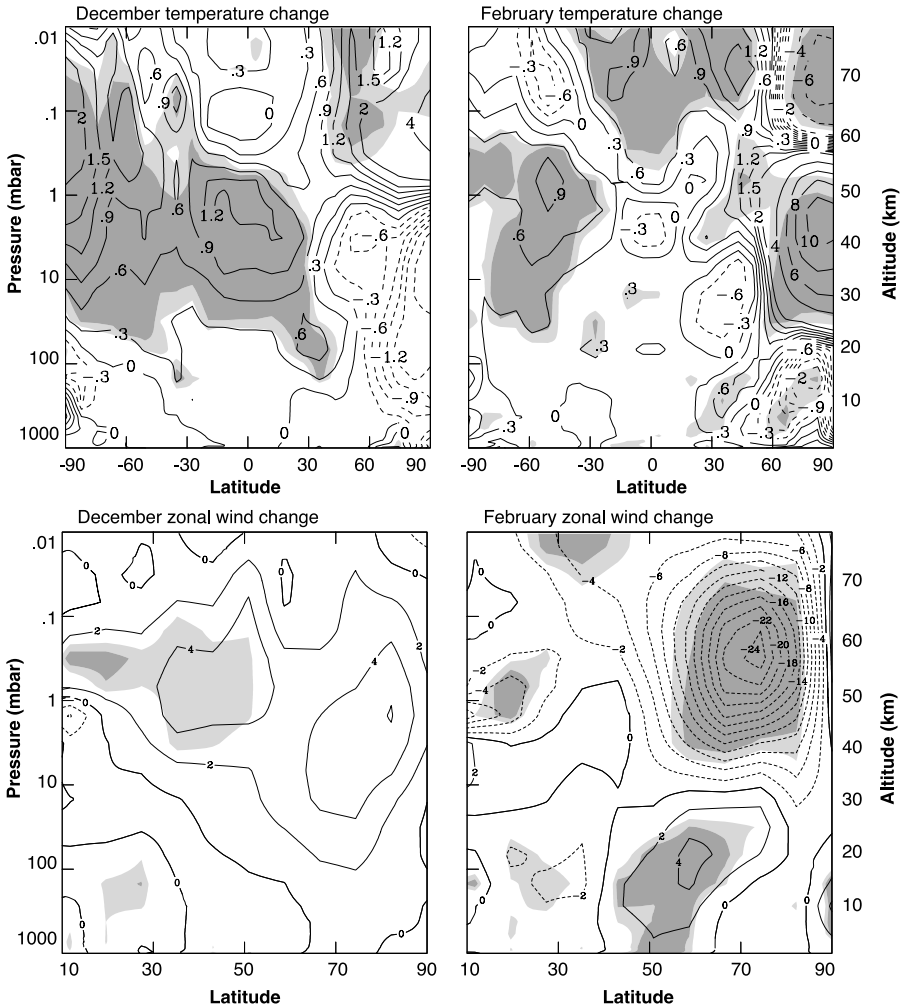

Fig. 5. Monthly modeled temperature differences (kelvin) and zonal wind changes (meters per second) between solar maximum and solar minimum for years without stratospheric warmings. The shading shows 90% (light) and 95% (dark) significance levels. Note that the upper and lower panels have different horizontal scales.

References and Notes

1. E. Friis-Christensen and H. Svensmark, *Adv. Space Res.* **20**, 913 (1997).
2. K. Labitzke and H. van Loon, *Space Sci. Rev.* **80**, 393 (1997).
3. M. Salby and D. J. Shea, *J. Geophys. Res.* **96**, 22579 (1991); S. Solomon *et al.*, *ibid.* **101**, 6713 (1996).
4. V. M. Mehta and T. Delworth, *J. Clim.* **8**, 172 (1995); G. R. Halliwell Jr., *ibid.* **10**, 2405 (1998).
5. M. A. Geller and J. C. Alpert, *J. Atmos. Sci.* **37**, 1197 (1980); J. D. Haigh, *J. Atmos. Solar Terr. Phys.* **61**, 63 (1999); N. F. Arnold and T. R. Robinson, *Ann. Geophys.* **16**, 69 (1998); K. Kodera, in *The Stratosphere and Its Role in the Climate System*, G. P. Brasseur, Ed. (NATO ASI Series I 54, Springer-Verlag, Berlin, 1997), pp. 83–98.
6. J. D. Haigh, *Science* **272**, 981 (1996).
7. J. L. Lean *et al.*, *J. Geophys. Res.* **102**, 29939 (1997).
8. R. T. Wetherald and S. Manabe, *J. Atmos. Sci.* **32**, 2044 (1975); E. Nesme-Ribes *et al.*, *J. Geophys. Res.* **98**, 18923 (1993); U. Cubasch *et al.*, *Clim. Dyn.* **13**, 757 (1997).
9. K. Kodera, K. Yamazaki, M. Chiba, K. Shibata, *Geophys. Res. Lett.* **17**, 1263 (1990).
10. N. K. Balachandran and D. Rind, *J. Clim.* **8**, 2058 (1995); D. Rind and N. K. Balachandran, *ibid.*, p. 2080.
11. J. Austin, N. Butchart, R. S. Swinbank, *Q. J. R. Meteorol. Soc.* **123**, 1405 (1997); D. Rind, D. Shindell, P. Lonergan, N. K. Balachandran, *J. Clim.* **11**, 876 (1998).
12. D. Shindell, D. Rind, P. Lonergan, *J. Clim.* **11**, 895 (1998).
13. Y. Naito and I. Hirota, *J. Meteorol. Soc. Jpn.* **75**, 925 (1997).
14. K. Labitzke, *Mon. Weather Rev.* **105**, 762 (1977); K. Kodera, M. Chiba, K. Shibata, *Geophys. Res. Lett.* **18**, 1209 (1991).
15. J. P. McCormack, L. L. Hood, R. D. McPeters, *Geophys. Res. Lett.* **24**, 2729 (1997).
16. L. L. Hood, *J. Geophys. Res.* **102**, 1355 (1997).
17. G. Brasseur, *ibid.* **98**, 23079 (1993); J. D. Haigh, *Nature* **370**, 544 (1994); E. L. Fleming *et al.*, *J. Atmos. Terr. Phys.* **57**, 333 (1995).
18. J. P. McCormack and L. L. Hood, *J. Geophys. Res.* **101**, 20933 (1996).
19. S. Chandra *et al.*, *Geophys. Res. Lett.* **23**, 2935 (1996).
20. The vertical shear is important further poleward and at higher levels, where wave refraction changes lead to convergence and heating in the upper stratosphere in January and February (Fig. 5).
21. K. Kodera, *J. Geophys. Res.* **100**, 14077 (1995).
22. World Meteorological Organization, *Scientific Assessment of Ozone Depletion: 1994* (Rep. 37, Global Ozone Res. and Monit. Proj., Geneva, 1994).
23. The two analyses are not statistically different at any latitude.
24. D. Rind, N. K. Balachandran, R. Suozzo, *J. Clim.* **5**, 189 (1992).

25. We thank K. Labitzke for providing data and G. A. Schmidt for comments. Supported by NASA's Solar Influence on Global Change Research and Analysis Program, NASA's Atmospheric Chemistry Modeling and Analysis Program, NASA's UARS Guest Investigator Program, and NSF's Solar Terrestrial Physics Program.

14 January 1999; accepted 8 March 1999